# UWB Sequential Monte Carlo Positioning using Virtual Anchors

Paul Meissner*, Thomas Gigl*,° and Klaus Witrisal*
*Graz University of Technology, Graz, Austria. Email: {paul.meissner, thomas.gigl, witrisal}@tugraz.at
°CISC Semiconductor, Design and Consulting GmbH, Austria

***Abstract*—We present a novel UWB indoor localization concept that performs the position estimation with a set of virtual anchor nodes, generated from a single physical anchor and floor plan information. Using range estimates to the virtual anchors, we perform multilateration to estimate the position of an agent. Previous work has shown the general applicability of this concept. In this contribution, we use a moving agent to exploit the correlation in successive positions using state-space concepts. A motion model for the agent and the measurement likelihood function allow for the use of the powerful framework of Bayesian state estimation. With this concept, we can propagate prior information on the agent position from one time step to the next. The statistical model for the ranging to the virtual anchors accounts for several imperfections, which lead to multimodal and heavy-tailed measurement distributions. We show how modified versions of the Kalman filter as well as a particle filter can account for these imperfections and yield accurate and robust position estimates. In a typical indoor pedestrian motion scenario, we can achieve an accuracy of about 45 cm for 90% of the estimates.**

## I. Introduction

In previous work [1], we have shown how an agent can be localized using ultra-wideband (UWB) radio signals transmitted between the agent and a single anchor node at a known location. Our approach exploits the multipath components (MPCs) of the UWB signal, which result from signal reflections at e.g. the room walls. Using given floor plan information, these MPCs can be mapped to virtual anchors (VAs), which are mirror images of the anchor with respect to the room walls, or other reflecting surfaces. Fig. 1 shows a scenario with VAs corresponding to single and double wall reflections. The locations of the VAs can be easily computed with the help of the floor plan. From the UWB channel impulse response (CIR), range estimates to the VAs can be obtained. The position of the agent can then be computed from these range estimates using statistical techniques.

As we have shown in [1], the availability of prior information about the agents position results in a potentially accurate and robust position estimator. In this contribution, we consider a moving agent, like the one shown in Fig. 1. The sequence of its positions will be correlated in time. Using appropriate techniques like state-space motion models and the corresponding estimation techniques, we can propagate position knowledge from one time step to the next. In this manner, previous position estimates can be used as prior knowledge.

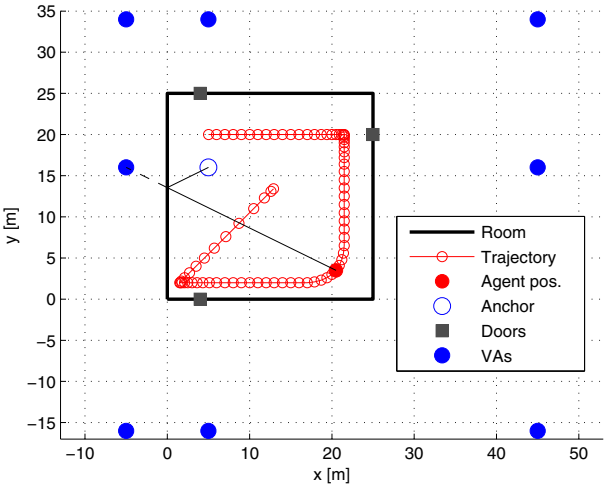


Fig. 1. Indoor positioning scenario with example room geometry and movement trajectory. There is only one physically existing anchor node, VA locations can be computed from the floor plan. Single- and double-reflection VAs are shown. The length of the single-reflection path from the anchor to the agent along the left wall equals the agents distance to the respective VA.

We show that the ubiquitous standard Kalman filter [2] is not useful for our approach, as our statistical models can either be multimodal or show heavy tails. There are numerous variants of the Kalman filter that account for such scenarios, e.g. [3], [4]. We will use a modified version of the Kalman filter that allows to alleviate measurement outliers. This filter needs a good and robust initialization, for which we propose a variant of the Gaussian sum filter [3]. To make full use of our specified statistical models, we use Bayesian filtering techniques [5]–[7]. Such techniques have often been successfully applied for localization, e.g. in [8] for tracking in UWB radar sensor networks.

We make explicit use of signal reflections together with floor plan information. The latter is often used only to truncate the search area, while e.g. in [9] such information is also used to discard invalid particle paths in a Bayesian filtering context. Reflected signal paths are often only seen as impairments that can lead to biased range estimates in non-line-of-sight (NLOS) scenarios. There is few work that actually exploits this information: [10] uses NLOS paths, with the need to estimate

This work was partly supported by the Austrian Science Fund (FWF) within the National Research Network SISE project S10604-N13 and by the Austrian Research Promotion Agency (FFG) under grant number 814560 (COMAR).

978-1-4244-5864-6/10$26.00 © IEEE

not only range-, but also angular information of these paths, which leads to a potentially complex receiver. Single-bounce paths are also used in [11], where in addition to the angular parameters, also the Doppler shift is estimated. For an UWB link with single antennas on both link ends, [12] proposes an algorithm for anchor-less localization, but with an assumed LOS situation and a fixed number of multipaths. The concept of virtual anchors is also used in [13], where the reflections result in new nodes at unknown locations that contribute in the location estimation through cooperation. In [14], reflections from an UWB signal are used for imaging purposes, which corresponds to the well-known simultaneous localization and mapping problem.

The extraction of multipath components is a key step of our approach and is as such still ongoing work [15]. However, for MPC extraction, a wealth of publications exists, e.g. [16], [17]. Our approach combines the knowledge of the floor plan with the information embedded in the structure of the CIR to turn one anchor node into a set of VAs that provides rich localization information.

This paper is organized as follows: Section II introduces the mathematical and statistical models that are used, Section III discusses in detail the state-space estimation algorithms that were adapted to our problem. Finally, Section IV presents performance results and Section V draws conclusions and mentions important future and ongoing work.

Throughout the paper, column vectors are boldface and lowercase, matrices are boldface and uppercase, $\mathbf{x}^T$ denotes the transposition of the vector $\mathbf{x}$ and $\hat{\mathbf{x}}_k$ indicates an estimate of $\mathbf{x}_k$ at the discrete time step $k$. A multivariate normal distribution for the random vector $\mathbf{x}$ with mean vector $\mathbf{m}$ and covariance matrix $\mathbf{\Sigma}$ is denoted by $\mathcal{N}(\mathbf{x}|\mathbf{m}, \mathbf{\Sigma})$

## II. Localization using virtual anchors

Using UWB signals, many of the reflected signal paths within a room are resolvable. For example, Fig. 2 shows an UWB CIR measured in a very recent campaign. It is well-known that such a CIR consists of a sum of delayed and scaled (and possibly distorted) copies of a transmitted pulse [18], which is well visible. A key step of our approach is to extract the delays of the MPCs, that correspond to the VAs from such a CIR. Using these delays, we can perform multilateration to estimate the agents position.

### A. Static location estimation using VAs

The result of the MPC extraction step is a vector $\mathbf{z}$ containing range estimates to the VAs. As discussed in detail in [1], we have to take several possible imperfections of this step into account: First, $\mathbf{z}$ can contain entries that are not caused by an MPC (false positive detections), second, some reflected paths could be missed by the detection and third, we do not assume that the entries are mapped to the corresponding VAs. Because of these imperfections, we call $\mathbf{z}$ a pseudodistance vector.

We have shown that a probabilistic model for one entry $z_i$ of the pseudodistance vector $\mathbf{z}$ can be given as a likelihood

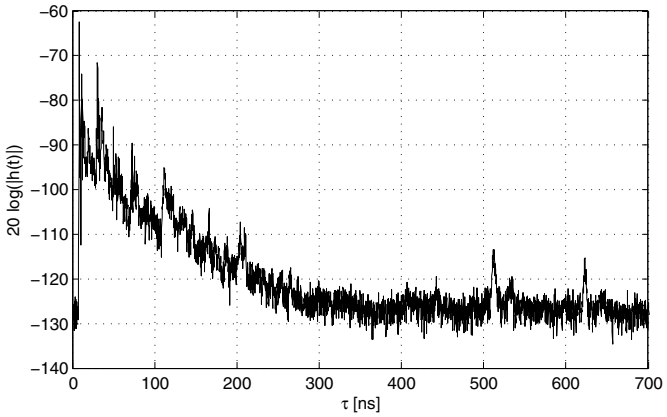


Fig. 2. Example for an UWB impulse response from a recent measurement campaign. Reflected paths are well visible as peaks over the noise floor.

function parameterized with the position $\mathbf{p}$

$$\begin{aligned} p_{z_i|\mathbf{p}}(z_i|\mathbf{p}) &= P_{\mathrm{VA}} \frac{1}{\sum_{n=1}^{N_{\mathrm{VA}}} v_n} \sum_{n=1}^{N_{\mathrm{VA}}} v_n \mathcal{N}(z_i \mid ||\mathbf{p}-\mathbf{p}_n||, \sigma_n^2) \\ &+ (1-P_{\mathrm{VA}}) p_{z_i,\overline{\mathrm{VA}}|\mathbf{p}}(z_i|\mathbf{p}) \end{aligned} \quad (1)$$

where $P_{\mathrm{VA}}$ is the probability that a $z_i$ corresponds to a VA and $v_n$ is the probability that the $n$-th VA at position $\mathbf{p}_{\mathrm{n}}$ is visible. $N_{\mathrm{VA}}$ is the number of VAs that are taken into account. Here, we use the direct signal path as well as single and double reflections, hence $N_{\mathrm{VA}} = 9$. The PDF $p_{z_i,\overline{\mathrm{VA}}|\mathbf{p}}(z_i|\mathbf{p})$ is the distribution of a $z_i$ that resulted from a false detection. We select this PDF as a uniform distribution between zero and a maximum range value that is larger than the possible domain of VA-matched $z_i$. The distance estimates to the VAs follow a normal distribution around their true values $||\mathbf{p}-\mathbf{p}_n||$ with a variance $\sigma_n^2$.

Assuming statistical independence of the $N$ pseudodistances $z_i$, the joint likelihood function of $\mathbf{z}$ can be expressed as

$$p_{\mathbf{z}|\mathbf{p}}(\mathbf{z}|\mathbf{p}) = \prod_{i=1}^{N} p_{z_i|\mathbf{p}}(z_i|\mathbf{p}) \quad (2)$$

An example for the log-likelihood $\ln\big(p_{\mathbf{z}|\mathbf{p}}(\mathbf{z}|\mathbf{p})\big)$ is shown in Fig. 3. We can observe that this functions shows a multimodal behavior, which is a result of the imperfections that it accounts for. A maximum-likelihood (ML) location estimate is given by

$$\hat{\mathbf{p}}_{\mathrm{ML}} = \begin{bmatrix} \hat{p}_x \\ \hat{p}_y \end{bmatrix}_{\mathrm{ML}} = \arg\max_{\mathbf{p}} p_{\mathbf{z}|\mathbf{p}}(\mathbf{z}|\mathbf{p}) \quad (3)$$

Performance results in [1] have shown that using this ML technique results in a potentially accurate, but not very robust estimator, as it contains large outliers. This is confirmed by Fig. 4, which shows a histogram of the ML position estimation error in the $x$-direction, $\mathrm{Err}_{\hat{\mathbf{p}},\mathrm{x,ML}} = p_{x,\mathrm{RX}} - \hat{p}_{x,\mathrm{ML}}$. We can observe that the estimator is unbiased but follows a heavy-tailed distribution. Assuming availability of prior information on the agents position substantially increased the robustness. The next subsection explains how to actually obtain this prior information.

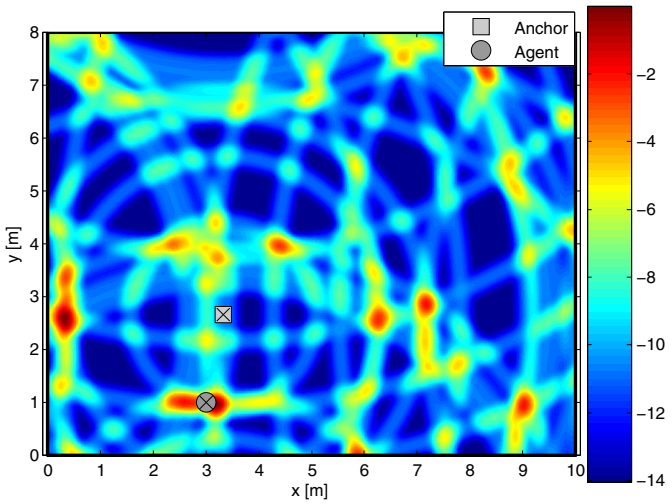


Fig. 3. Plot of measurement log-likelihood $\ln\big(p_{\mathbf{z}|\mathbf{p}}(\mathbf{z}|\mathbf{p})\big)$ for one specific realization of $\mathbf{z}$ containing 5 VA-matched $z_i$ and 5 false detections. In this case, the likelihood function is multimodal and the ML estimation chooses the wrong mode near $\mathbf{p} = [0.5,\ 2.5]^T$.

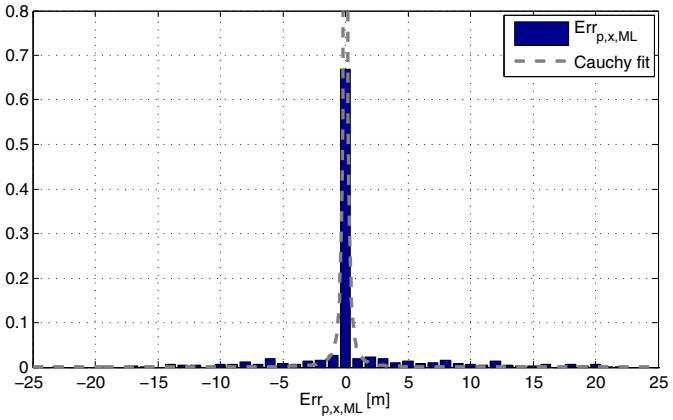


Fig. 4. Normalized histogram of position error in the $x$ coordinate of the ML-estimate. The histogram indicates that this error follows a heavy-tail distribution. The grey dashed line is a fit of a Cauchy distribution to the ML error in the $x$-direction. The $y$-direction is distributed analogously.

### B. Localization of a moving agent

Let us assume we want to track the position of a moving agent in a room with known geometry. For the mathematical description, we will use a standard state-space model of the movement. We will consider a two-dimensional discrete-time model with time index $k$ and a sampling time of $\Delta T$. The state vector of the mobile agent at time $k$ is defined as $\mathbf{x}_k = [p_x, p_y, v_x, v_y]_k^T$; it contains position and velocity in $x$ and $y$ directions. In general, a state-space model is defined by the two equations

$$\mathbf{x}_{k+1} = f_k(\mathbf{x}_k, \boldsymbol{\omega}_k) \tag{4}$$

$$\mathbf{y}_k = h_k(\mathbf{x}_k, \boldsymbol{\nu}_k) \tag{5}$$

where (4) is called the system- or state-propagation equation. It maps a state vector from one time step to the next, where $\boldsymbol{\omega}_k$ denotes the the process noise [2]. The state vector itself is only accessible via the function $h_k(\mathbf{x}_k)$, which is therefore called the measurement equation. The vector $\boldsymbol{\nu}_k$ is the measurement noise.

A possible scenario is shown in Fig. 1. A movement like this can be described with a well-known linear dynamical motion model [19], [20]

$$\mathbf{x}_{k+1} = \underbrace{\begin{bmatrix} 1 & 0 & \Delta T & 0 \\ 0 & 1 & 0 & \Delta T \\ 0 & 0 & 1 & 0 \\ 0 & 0 & 0 & 1 \end{bmatrix}}_{\mathbf{F}} \mathbf{x}_k + \underbrace{\begin{bmatrix} \frac{\Delta T^2}{2} & 0 \\ 0 & \frac{\Delta T^2}{2} \\ \Delta T & 0 \\ 0 & \Delta T \end{bmatrix}}_{\mathbf{G}\mathbf{a}_k = \boldsymbol{\omega}_k} \mathbf{a}_k \tag{6}$$

where the function $f_k(\mathbf{x}_k) = f(\mathbf{x}_k)$ is linear and time-invariant. The vector $\mathbf{a}_k$ contains acceleration noise in $x$ and $y$ directions and is transformed in position and velocity noise components via multiplication with the matrix $\mathbf{G}$. This can be interpreted as process noise in the linear system. It can also be used as a deterministic driving input to the system, e.g. we used it to generate several different motion trajectories.

Concerning the measurement equation, we use two different types of measurements in this paper: First, we can take the ML position estimate at time step $k$, $\hat{\mathbf{p}}_{\mathrm{k,ML}}$ from (3) as an input to a state-space filter. Second, we can directly take the pseudodistances in $\mathbf{z}$. Both possibilities require some discussion, which follows next.

*1) Maximum likelihood estimates as measurements:* In this case we define the measurements as $\mathbf{y}_k = \hat{\mathbf{p}}_{\mathrm{k,ML}}$. Then we can write (5) as

$$\mathbf{y}_k = \underbrace{\begin{bmatrix} 1 & 0 & 0 & 0 \\ 0 & 1 & 0 & 0 \end{bmatrix}}_{\mathbf{H}} \mathbf{x}_k + \boldsymbol{\nu}_k \tag{7}$$

which, together with (6) is a linear state-space model, for which a standard Kalman filter would be applicable.

A Kalman filter is the optimal estimator in the minimum mean squared error sense for such a linear model if the noise terms are Gaussian. But a look at Fig. 4 suggests that this is not the case. A probabilistic model of the measurement error could be a sharply peaked unimodal, but heavy-tailed distribution. Approximating $\boldsymbol{\nu}_k$ as a zero-mean Gaussian noise term facilitates computations but fails to capture the large outliers. More appropriate heavy-tailed distributions can be obtained using the family of $\alpha$-stable distributions [21], for which the Cauchy distribution is a special case that has a closed-form PDF. Dropping the time index, a bivariate isotropic Cauchy distribution over the vector $\boldsymbol{\nu}$ with location parameter vector $\mathbf{m} = [m_x, m_y]^T$ and width parameter $\beta$ is denoted as $\mathcal{C}(\boldsymbol{\nu}|\mathbf{m}, \beta)$ and has the PDF [22]

$$p(\boldsymbol{\nu}) = \frac{\beta}{2\pi}\left[(\nu_x - m_x)^2 + (\nu_y - m_y)^2 + \beta^2\right]^{-3/2}. \tag{8}$$

Here, the width parameter $\beta$ is linked to the interquartile range [23] and the location parameters $m_x$ and $m_y$ are medians in $x$- and $y$-direction. Fig. 4 contains a fit of a Cauchy distribution

to $\mathrm{Err}_{\hat{\mathbf{p}},\mathrm{x,ML}}$ where $m_x = 0$ and $\beta$ is chosen as half the interquartile range of the error samples. We can also extend our noise model with the knowledge of the room dimensions. In this case, the distribution is a truncated bivariate isotropic Cauchy distribution which is defined as

$$\bar{\mathcal{C}}(\boldsymbol{\nu}|\mathbf{m},\beta) = \begin{cases} Z \cdot \mathcal{C}(\boldsymbol{\nu}|\mathbf{m},\beta) & |\nu_x| \leq d_x \text{ and } |\nu_y| \leq d_y \\ 0 & \text{otherwise.} \end{cases} \tag{9}$$

where $d_x$ and $d_y$ are the dimensions of the rectangular room. The normalization constant $Z$ ensures that $\bar{\mathcal{C}}(\cdot)$ is a proper PDF. As this is not important for the cases where we will actually use this distribution, we will drop the factor $Z$.

*2) Pseudodistance vector as measurement:* If we define the measurements as the pseudodistance vector, i.e. $\mathbf{y}_k = \mathbf{z}_k$, we do not end up at a deterministic closed-form measurement equation such as (7). This is due to the possible imperfections of the MPC-extraction discussed in Section II-A. If we have an estimate of the state vector $\hat{\mathbf{x}}_k$ available, then we can rate the plausibility of its position entries $\hat{\mathbf{p}}_k = \mathbf{H}\hat{\mathbf{x}}_k = [\hat{p}_x, \hat{p}_y]_k^T$ via the likelihood function given in (2) and (1). Hence, a likelihood for the measurements, given a position estimate $\hat{\mathbf{x}}_k$ can be given as

$$p(\mathbf{y}_k|\hat{\mathbf{x}}_k) = p_{\mathbf{z}|\mathbf{p}}(\mathbf{z}_k|\mathbf{p} = \mathbf{H}\hat{\mathbf{x}}_k) \tag{10}$$

We observe that in this case there is no deterministic measurement equation $h_k(\cdot)$. This is the consequence of a lack of a mapping of the $z_i$ to the VAs, and makes the application of Kalman-filter-like schemes impossible. Instead, we resort to Bayesian state-space estimation concepts and implement them using Particle filters. Those can deal with a purely probabilistic description of the measurements. Also, it is well-known that particle filters perform better than Kalman filters if the PDF of the measurements is multimodal in the domain of the state vector. As confirmed by Fig. 3, we have to deal with such a scenario.

A third possible choice concerning the measurements is to again take the pseudodistances and perform a mapping of its entries to the VAs. Then an extended Kalman filter using the range measurements would be applicable. Such a mapping scheme is subject of ongoing research.

## III. State space estimators

In the previous section we have shown that the virtual-anchor-based localization problem can be formulated as a standard state-space estimation problem. A block diagram of the overall system is shown in Fig. 5. The MPC extraction estimates a vector of distances to the VAs from the received UWB signal $r_k(t)$. This vector is processed by the static VA-based position estimation block, that computes the measurement likelihood function for $\mathbf{z}_k$ and an ML estimate. Both are passed to the state-space estimator that either uses the ML-estimate or $\mathbf{z}_k$ directly as its measurements. The different algorithms that can be used in the latter block are the subject of this subsection.

The state-space estimation problem can be solved using recursive Bayesian state estimation. Our aim is to estimate

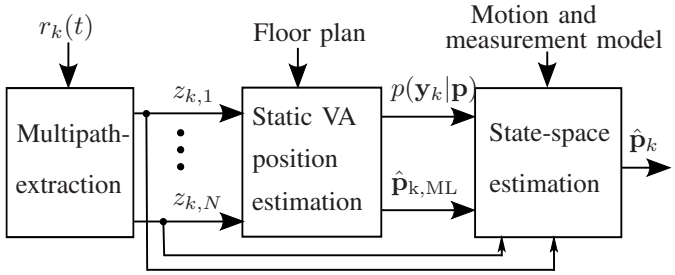


Fig. 5. Conceptual localization scheme at time $k$ using multipath extraction from the received signal $r_k(t)$, subsequent computation of the likelihood as a function of the position, followed by a state-space estimator. The latter can use either the ML-estimate or the likelihood function plus the pseudodistances as measurements.

the posterior distribution of the state vector $\mathbf{x}_k$, given all measurements up to and including time $k$. Denoting the latter set of measurements as $\mathbf{Y}_k$, this posterior PDF is written as $p(\mathbf{x}_k|\mathbf{Y}_k)$. It is well-known [2], [6], [7], that this problem can be solved using a sequence of prediction/update calculations. In the prediction step, we calculate the *a-priori* estimate of the PDF of $\mathbf{x}_k$

$$p(\mathbf{x}_k|\mathbf{Y}_{k-1}) = \int p(\mathbf{x}_k|\mathbf{x}_{k-1})p(\mathbf{x}_{k-1}|\mathbf{Y}_{k-1})d\mathbf{x}_{k-1} \tag{11}$$

which is the PDF of the state vector before taking the current measurement $\mathbf{y}_k$ into account. Equation (11) is known as the Chapman-Kolmogorov equation. In principle, it forms the new a-priori PDF of the state by using the transition density $p(\mathbf{x}_k|\mathbf{x}_{k-1})$ together with the posterior PDF from the previous time step $p(\mathbf{x}_{k-1}|\mathbf{Y}_{k-1})$ and marginalizing out the previous state vector.

At the time $k$, the new measurement is available and we can calculate the posterior PDF in the update step

$$p(\mathbf{x}_k|\mathbf{Y}_k) = \frac{p(\mathbf{y}_k|\mathbf{x}_k)p(\mathbf{x}_k|\mathbf{Y}_{k-1})}{\int p(\mathbf{y}_k|\mathbf{x}_k)p(\mathbf{x}_k|\mathbf{Y}_{k-1})d\mathbf{x}_k}. \tag{12}$$

Here, we need to evaluate the measurement likelihood $p(\mathbf{y}_k|\mathbf{x}_k)$ as well as the a-priori PDF from the prediction step. Both the transition density in the prediction step and the measurement likelihood in the update step can be obtained using probabilistic descriptions of (4) and (5) using the PDFs of the respective noise terms. To start the recursion, we need to select an initial guess of the state vector PDF $p(\mathbf{x}_0|\mathbf{Y}_0) = p(\mathbf{x}_0)$.

In theory, (11) and (12) give access to the full posterior PDF of the state vector. In practice, both equations can be solved analytically only for special cases, e.g. if the model and the measurement equation are linear and the noise terms are Gaussian. Then, the Kalman-filter is the optimal state-space estimator. In many other cases, we need to calculate approximations of the posterior PDF of the state. One possibility is to use a set of $N_p$ candidate state vectors, called *particles*, at which (11) and (12) are evaluated. The state-space estimators that we use in our localization scheme are the subject of the next section.

### A. Kalman filter with measurement refinement

Using a standard Kalman filter with the motion model in (6) and the ML-estimates of the position as measurements, i.e. (7), does not give satisfying results. Although both state-propagation and measurement equations are linear, the measurement noise is non-Gaussian as it contains large outliers.

We propose a modification of the standard Kalman filter that exploits the correlation of successive agent positions on a trajectory like shown in Fig. 1. For prediction and update phases, we use the standard Kalman filter equations [2]. The KF assumes that the PDF of the state vector is Gaussian and recursively estimates mean and covariance. We denote a-priori estimates with a minus and a-posteriori estimates with a plus in the superscript. The matrix $\mathbf{P}_k = \mathrm{E}\{(\mathbf{x}_k - \hat{\mathbf{x}}_k)(\mathbf{x}_k - \hat{\mathbf{x}}_k)^T\}$ is the estimation error covariance matrix and $\mathbf{Q_k}$ and $\mathbf{R_k}$ are the covariance matrices of process and measurement noise, respectively. Then, the KF equations are

$$\hat{\mathbf{x}}_k^- = \mathbf{F}\hat{\mathbf{x}}_{k-1}^+ \quad (13)$$

$$\mathbf{P}_k^- = \mathbf{F}\mathbf{P}_{k-1}^+\mathbf{F}^T + \mathbf{Q}_{k-1} \quad (14)$$

for the prediction phase of the Kalman filter, and

$$\mathbf{K}_k = \mathbf{P}_k^-\mathbf{H}^T(\mathbf{H}\mathbf{P}_k^-\mathbf{H}^T + \mathbf{R}_k)^{-1} \quad (15)$$

$$\mathbf{P}_k^+ = (\mathbf{I} - \mathbf{K}_k\mathbf{H})\mathbf{P}_k^-(\mathbf{I} - \mathbf{K}_k\mathbf{H})^T + \mathbf{K}_k\mathbf{R}_k\mathbf{K}_k^T \quad (16)$$

$$\hat{\mathbf{x}}_k^+ = \hat{\mathbf{x}}_k^- + \mathbf{K}_k(\mathbf{y}_k - \mathbf{H}\hat{\mathbf{x}}_k^-) \quad (17)$$

for the update phase.

Our variant of the Kalman filter modifies the measurement $\mathbf{y}_k$ given in (7) to reduce the outliers. Under the assumption that $\mathbf{x}_{k-1}^+$ represents a relatively "good" estimate of the state vector, we can expect that $\mathbf{x}_k$ will be in the vicinity of it, bounded by the finite velocity of the agent. Hence we define a Gaussian position prior centered at the predicted position $\hat{\mathbf{p}}_k^- = \mathbf{H}\hat{\mathbf{x}}_k^-$ as

$$p_k(\mathbf{p}) = \mathcal{N}(\mathbf{p} \mid [\hat{p}_{x,k}^-, \hat{p}_{y,k}^-]^T, \sigma_p^2). \quad (18)$$

The prior variance $\sigma_p^2$ is a design parameter that should be chosen such that it allows for a movement with the expected maximum of the velocity. The actual measurement used in the update phase of the KF is then obtained by replacing the ML-position estimate with a MAP-estimate

$$\mathbf{y}_k = \arg\max_{\mathbf{p}} p_k(\mathbf{p}) p_{\mathbf{z}|\mathbf{p}}(\mathbf{z}|\mathbf{p}) \quad (19)$$

where the prior attenuates incorrect maxima of the multimodal measurement likelihood function of the pseudodistance vector.

The assumption of a reasonably good estimate from the previous time step boils down to a careful initialization of the algorithm with proper $\hat{\mathbf{x}}_0^+$ and $\mathbf{P}_0^+$. An outline of the algorithm is described in Table I.

### B. Initialization – Gaussian sum filter

In the KF with measurement refinement, a correct initialization of the algorithm is crucial, as the prediction using the initial state vector defines the mean of the first position prior. In practice, the initialization using this algorithm can be done in the following way: Instead of following just one state trajectory hypothesis, we use multiple weighted hypotheses. This can be done using the concept of a Gaussian sum filter (GSF) [3], where the state vector posterior PDF is represented by a Gaussian mixture of the form

$$p(\hat{\mathbf{x}}_k^+) = \sum_{i=1}^{M} a_{k,i}\mathcal{N}(\mathbf{x}_k \mid \hat{\mathbf{x}}_{k,i}^+, \mathbf{P}_{k,i}^+). \quad (20)$$

In principle, this is equivalent to a bank of $M$ parallel Kalman filters, where we will use our modified KF from the previous section. To choose the weights $a_{k,i}$, we look at the *innovation* process of each KF. It is defined as the term in the brackets on the right hand side of (17)

$$\mathbf{r}_{k,i} = \mathbf{y}_{k,i} - \mathbf{H}\hat{\mathbf{x}}_{k,i}^- \quad (21)$$

According to theory [2], this should be a zero-mean Gaussian white noise process with covariance matrix $\mathbf{H}\mathbf{P}_{k,i}^-\mathbf{H}^T + \mathbf{R}_{k,i}$. Hence, a relative confidence measure of the estimate of each KF can be computed as

$$\beta_{k,i} = \mathcal{N}(\mathbf{r}_{k,i} \mid \mathbf{0}, \mathbf{H}\mathbf{P}_{k,i}^-\mathbf{H}^T + \mathbf{R}_{k,i}). \quad (22)$$

Subsequently the weights $a_{k,i}$ are obtained as in [3]

$$a_{k,i} = \frac{a_{k-1,i}\beta_{k,i}}{\sum_{j=1}^{M} a_{k-1,j}\beta_{k,j}}. \quad (23)$$

The original motivation of the GSF was to represent a non-Gaussian state vector PDF by a combination of all $M$ KFs using (20). Our intention is to just represent $M$ state vector hypotheses and find the one closest to the true trajectory with the help of the $a_{k,i}$. Simulations showed that the KFs that are initialized rather far away from the true trajectory have quickly decaying weights and could in principle also be discarded after the initialization phase. To draw our state vector estimate, we do not combine the KFs, we just take the $\hat{\mathbf{x}}_{k,i}^+$ with the maximum corresponding weight.

The algorithm is outlined in Table II. It can handle the initialization problem as follows: At $k = 0$, the $M$ initial state vectors are chosen. We identify two scenarios, depending on our prior knowledge. The first case corresponds to a scenario where we do not know anything about the initial agent position, so we choose the initial positions randomly, according to a uniform distribution bounded by the room dimensions. The initial velocities are set to zero. In the second

TABLE I
KALMAN FILTER WITH MEASUREMENT REFINEMENT

@$k = 0$ **do:** Choose initial estimates $\hat{\mathbf{x}}_0^+$ and $\mathbf{P}_0^+$
**for all** $k > 0$ **do**
  **procedure** KALMANREF($\mathbf{x}_{k-1}^+, \mathbf{P}_{k-1}^+$)
    Predict $\hat{\mathbf{x}}_k^-$ and $\mathbf{P}_k^-$ using (13) and (14)
    Set up position prior $\mathcal{N}(\mathbf{p} \mid [\hat{p}_{x,k}^-, \hat{p}_{y,k}^-]^T, \sigma_p^2)$
    Select refined measurement $\mathbf{y}_k$ according to (19)
    Calculate $\hat{\mathbf{x}}_k^+$ and $\mathbf{P}_k^+$ as in (15), (16) and (17)
    **return** $\hat{\mathbf{p}}_k = \mathbf{H}\hat{\mathbf{x}}_k^+$
  **end procedure**
**end for**

TABLE II
GAUSSIAN SUM FILTER

@$k = 0$ **do**
**for all** $i = 1..M$ **do**
  Set $a_{0,i} = 1/M$
  Choose initial estimates $\hat{\mathbf{x}}^+_{0,i}$ and $\mathbf{P}^+_{0,i}$
**end for**
**for all** $k > 0$ **do**
  **procedure** GSF($\{\mathbf{x}^+_{k-1,i}, \mathbf{P}^+_{k-1,i}, a_{k-1,i}\}_{i=1}^M, M$)
    **for all** $i = 1..M$ **do**
      Perform KALMANREF($\mathbf{x}^+_{k-1,i}, \mathbf{P}^+_{k-1,i}$)
    **end for**
    Update weights $\{a_{k,i}\}_{i=1}^M$ using (23)
    Select $i_{\max} = \arg\max_i \{a_{k,i}\}$
    **return** $\hat{\mathbf{p}}_k = \mathbf{H}\hat{\mathbf{x}}^+_{k,i_{\max}}$
  **end procedure**
**end for**

case, we assume that we are monitoring movement within a room and we set the initial positions equal to the known locations of the room doors, where $M$ equals the number of doors. The initial velocities can be selected such that they point in a direction orthogonal to the corresponding wall and inside the room, to represent the entry through this door.

### C. Particle filter

Both the KF with refined measurements and the GSF are variants of the Kalman filter, that treat the measurement noise as Gaussian. Although the measurement refinement procedure should decrease the influence of large outliers of the ML-estimate, it does not model the measurement noise term correctly as we have seen in Section II-A. Also, we still want to obtain a state-space estimator that uses the pseudodistance vector $\mathbf{z}_k$ and the associated likelihood function (2) directly. Both objectives can be handled using particle filters, which are an implementation of the recursive Bayesian state estimator in (11) and (12) using Monte Carlo techniques. Therefore, they belong to the family of sequential Monte Carlo algorithms [6], [7].

A PF uses a set of $N_p$ particles (candidate state vectors) and corresponding weights. Our chosen PF variant corresponds to a sampling-importance-resampling (SIR) PF, where resampling is performed at every time step. After the update phase at each time step $k$ the particles are distributed according to the state posterior PDF $p(\mathbf{x}_k|\mathbf{Y}_k)$. The set of a-priori particles, obtained by using (4) at time $k$, is denoted as $\{\hat{\mathbf{x}}^-_{k,i}\}_{i=1}^{N_p}$ and the set of weights as $\{w_{k,i}\}_{i=1}^{N_p}$. In the update phase, the measurement $\mathbf{y}_k$ is taken into account. This is done by evaluating the likelihood of the measurement, given each particle. These likelihoods are the weights of the particles, which are then normalized such that they sum up to one. The last step is the resampling of the particles, which results in the posterior particles, which are denoted by a plus in the superscript. The resampling is done by drawing the particles with replacement from the multinomial distribution over the a-priori particles, with probabilities given by the weights. After resampling, the weights are reset to a value of $1/N_p$.

The advantage of using a PF is, that it allows for a more appropriate statistical modeling of noise PDF and measurement likelihood function. These statistical descriptions have been outlined in Section II-B. We now briefly discuss the different phases of our PF, an algorithm outline is found in Table III.

*1) Initialization phase:* The initialization of the PF can be done similar to the GSF in the previous subsection: One possibility is to select the position entries of the initial particles uniformly distributed within the room, with the velocities at zero. Another possibility is to sample the positions of the initial particles from a mixture of $M$ (equal to the number of doors) truncated bivariate Gaussians, each one centered at the position of one of the room doors. In simulations, choosing the door initialization did not lead to a considerable gain in performance. The PF was able to rapidly lock on the trajectory also with the complete random initialization.

*2) Prediction phase of the PF:* At each time step $k$, a set of new a-priori particles $\{\hat{\mathbf{x}}^-_{k,i}\}_{i=1}^{N_p}$ is obtained by passing the posterior particles from $k-1$ through the state propagation equation (4). Here, the linear motion model (6) is used and the noise term $\mathbf{a}_k$ is a zero-mean Gaussian with covariance $\mathbf{I}\sigma_a^2$. Hence, the a-priori particles are distributed as

$$\hat{\mathbf{x}}^-_{k,i} \sim \mathcal{N}(\mathbf{x}^-_{k,i} \mid \mathbf{F}\hat{\mathbf{x}}^+_{k-1,i}, \sigma_a^2\mathbf{G}\mathbf{G}^T),\ i \in \{1 \dots N_p\} \quad (24)$$

i.e. they follow a Gaussian distribution, from which they can be sampled conveniently. The variance $\sigma_a^2$ has to be chosen large enough such that a change in movement with the highest expected acceleration is possible.

*3) Update phase: ML measurements and Cauchy likelihood:* As we have seen in Fig. 4, the measurement noise term can be modeled using a truncated bivariate isotropic Cauchy distribution $\bar{\mathcal{C}}(\cdot)$ for $\mathbf{y}_k = \hat{\mathbf{p}}_{\mathrm{k,ML}}$. Using the PF, we can easily model this behavior. The weights of the particles are computed as the value of $\bar{\mathcal{C}}(\cdot)$ centered at the ML-estimate evaluated at the position coordinates of the particles

$$w_{k,i} = \bar{\mathcal{C}}(\mathbf{H}\mathbf{x}^-_{k,i} \mid \hat{\mathbf{p}}_{\mathrm{,k,ML}}, \beta). \quad (25)$$

This distribution differs from the definition in (9) in the truncation: Here, $\bar{\mathcal{C}}(\cdot)$ is only non-zero if both $x$ and $y$ coordinates of the particle are within the room. With this definition, particles outside the room are automatically discarded as their weight will be zero and therefore also the probability of resampling. The width $\beta$ is a design parameter that can be chosen as outlined in section II-B1.

*4) Update phase: Pseudodistance measurements and likelihood model:* Here, $\mathbf{y}_k = \mathbf{z}_k$ and the likelihood function for the particles is given in (2) and (1)

$$w_{k,i} = p_{\mathbf{z}|\mathbf{p}}(\mathbf{z}_k|\mathbf{H}\hat{\mathbf{x}}^-_{k,i}). \quad (26)$$

Also this function is zero for a position coordinate outside the room.

*5) Location estimation using the posterior particles:* The next step is to resample the particles according to their weights. The step results in the posterior particles, that are distributed according to the state vector posterior PDF. Hence, any desired

TABLE III
PARTICLE FILTER WITH ML-POSITION- OR PSEUDODISTANCE-MEASUREMENTS

@$k = 0$ **do** Select initial set of particles $\{\hat{\mathbf{x}}_{0,i}^{+}\}_{i=1}^{N_p}$
**for all** $k > 0$ **do**
  **procedure** PF($\{\mathbf{x}_{k-1,i}^{+}\}_{i=1}^{N_p}, \hat{\mathbf{p}}_{\mathrm{k,ML}}, \mathbf{z}_k$)
    **for all** $i = 1 \leq N_p$ **do**
      Sample a-priori particle $\hat{\mathbf{x}}_{k,i}^{-}$ according to (24)
      **if** $\mathbf{y}_k = \hat{\mathbf{p}}_{\mathrm{k,ML}}$ **then** ▷ ML-estimates
        Evaluate weight $w_{k,i}$ as in (25)
      **else if** $\mathbf{y}_k = \mathbf{z}_k$ **then** ▷ pseudodistances
        Evaluate weight $w_{k,i}$ as in (26)
      **end if**
    **end for**
    Normalize weights
    Resample particles to get $\{\hat{\mathbf{x}}_{k,i}^{+}\}_{i=1}^{N_p}$
    **return** $\hat{\mathbf{p}}_k = \mathrm{median}(\{\mathbf{H}\hat{\mathbf{x}}_{k,i}^{+}\}_{i=1}^{N_p})$
  **end procedure**
**end for**

estimate can be approximated. In performance simulations, we observed that the median of each component yields satisfying results. This is due to the fact that the median is more robust to clouds of particles that correspond to outliers than the mean. Such outliers can be the result of particles that are resampled at wrong modes of the multimodal range likelihood function. Choosing the median of the posterior distribution corresponds to a minimization of the absolute error [24].

## IV. PERFORMANCE RESULTS

For performance simulations, we selected typical indoor localization scenarios. A scenario consists of a trajectory, that is a sequence of agent positions and velocities, as well as a given room geometry and the position of the single anchor node. One is the trajectory shown in Fig. 1, the other one is shown in Fig. 6. The scenarios represent indoor pedestrian movement at varying velocity. In these simulations, the anchor node is used and denoted as the transmitter (TX), but the roles of TX and and receiver (RX) can of course also be reversed.

The parameters of the statistical model for the pseudodistance vector in (1) have been set as follows: We chose $P_{\mathrm{VA}} = 0.5$, which means that we expect half of the $z_i$ in one MPC-extraction process to be false detections. The visibilities of the VAs $v_n$ are chosen such that the LOS path, the single reflection VAs and the double reflection VAs are visible with probabilities of 0.8, 0.5 and 0.3, respectively. It should be noted, that the actual visibilities are drawn independently for each position of the RX, which could correspond to a scenario with lots of additional scatterers like furniture or moving people. Correlation of the visibilities over time are subject of current research. The standard deviation of the distance estimates to the VAs, $\sigma_n$ has been selected as 10 cm.

Fig. 7 shows the CDF of the position estimation error $\mathrm{Err}_{\hat{\mathbf{p}}} = ||\mathbf{p}_{\mathrm{RX}} - \hat{\mathbf{p}}||$ for 50 simulated runs over the trajectory shown in Fig. 6. On average, the PF with the pseudodistance measurements shows the best performance. About 90 % of the estimates are within 43 cm. Also its error floor is small and is just due to the random initialization. The other estimators

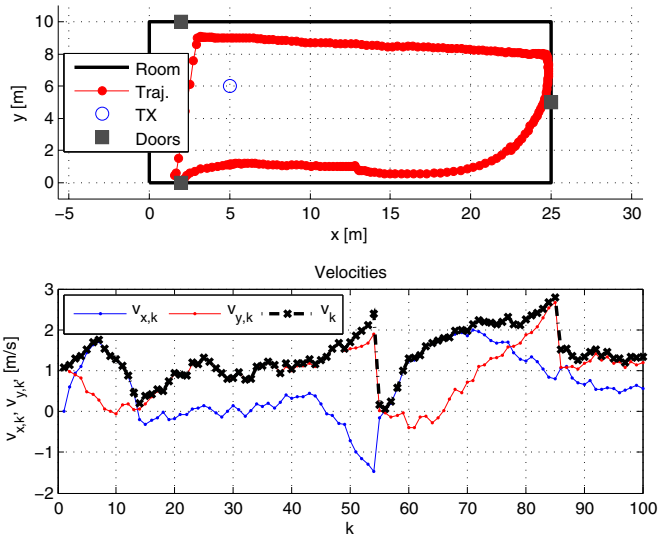


Fig. 6. Indoor pedestrian motion scenario. Top plot shows the sequence of 245 positions in the room and the lower plot shows the velocity components for $k \leq 100$. A pedestrian enters the room through the door in the south-west and then walks along the walls with varying velocity, including some stops. This could model a maintenance worker or a visitor in a museum gallery.

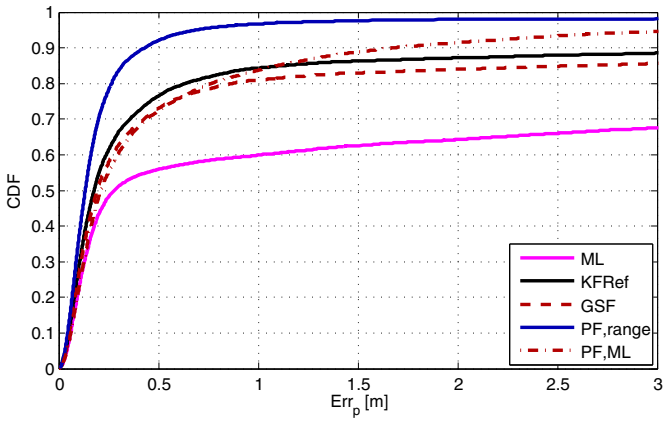


Fig. 7. CDF of the position errors for 50 runs over the trajectory in Fig. 6. The average behaviour of the estimators can be observed.

show a substantially better performance than the ML-estimate, on which all of them are based. Their error floor is caused by occasional divergence of the KF and the GSF. It is well-known that Kalman filters can diverge if model assumptions do not hold, which in our case corresponds to the non-Gaussian measurement noise. In this scenario, five of the 50 runs showed diverging results. In case of the PF with ML-measurements, the error floor is caused by the fact that this estimator is still influenced by the ML-outliers, though much less than a standard KF. Taking the pseudodistances as measurements is seemingly the best way to deal with the multimodality of the likelihood function (2). This is due to the fact that the decision for the correct mode is here in the responsibility of the tracking algorithm, and not the ML-estimation based on just the current time step.

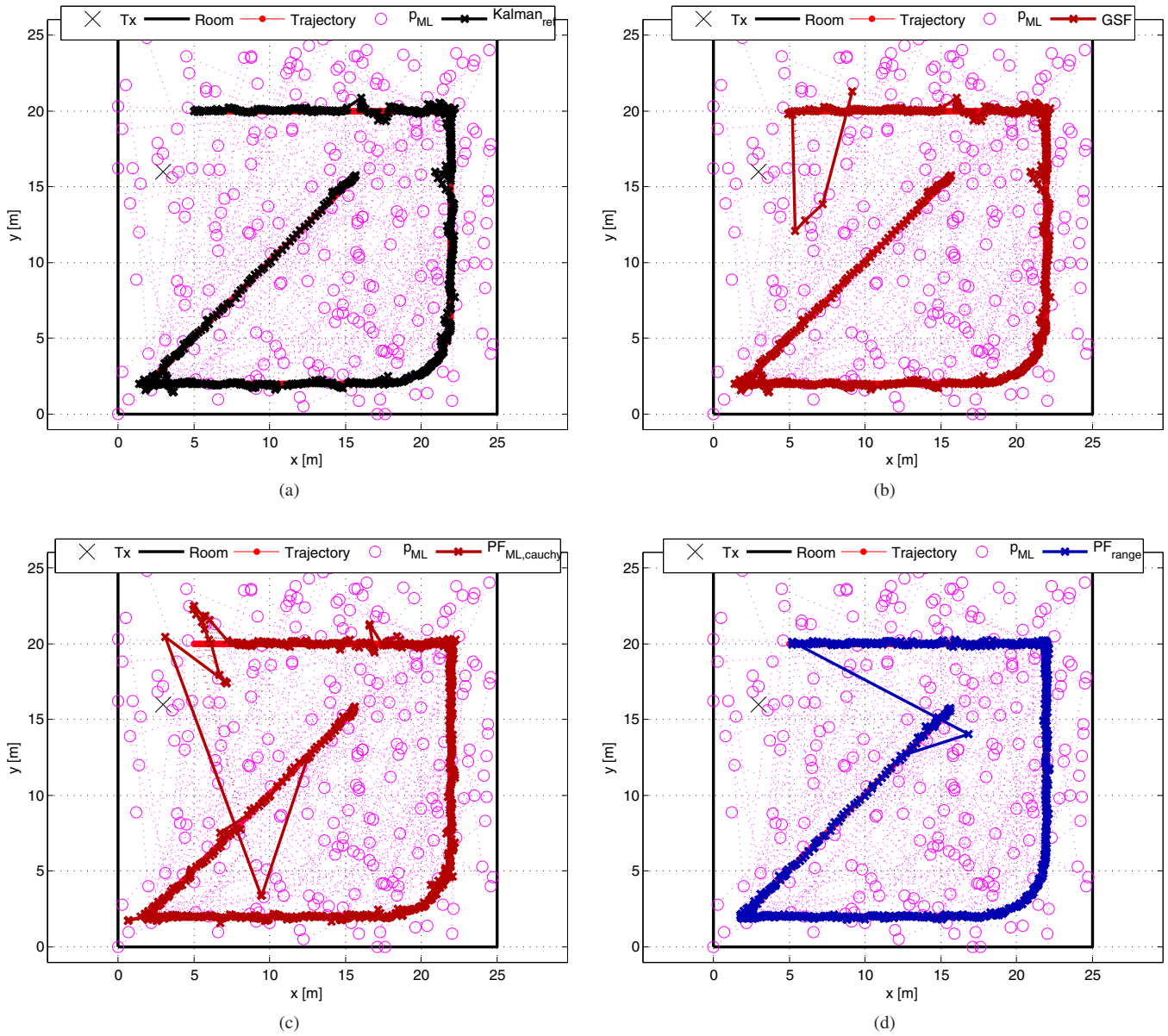


Fig. 8. Performance results for the four state-space filters over the trajectory from Fig. 1, starting point is in the north-west. Magenta circles are outliers of the ML-estimates ($\mathrm{Err}_{\hat{\mathbf{p}}\mathrm{ML}} > 1$ m). The dotted lines connect the ML-estimates to their respective true positions. (a) Kalman filter with measurement refinement and perfect initialization. (b) Gaussian sum filter with $M = 10$ uniformly random selected components. (c) Particle filter with ML-estimates and Cauchy error model and $N_p = 2000$ particles. (d) Particle filter with pseudodistances and $N_p = 2000$ particles.

A comparison of all four estimators for the scenario in Fig. 1 can be found in Fig. 8 and 9 . This scenario supports the previous results from e.g. Fig. 7, i.e., KF with measurement refinement and GSF show similar performance. The KF is initialized here with the true initial state vector, while the GSF draws $M = 5$ random initial state vectors. It converges quickly to the correct trajectory. The PF with the ML-estimates as measurements is again more influenced by their outliers than the one using pseudodistances. Both PFs use $N_p = 2000$ particles. Increasing this number leads to better robustness. Concerning the initialization, both PFs use particles that are randomly drawn according to a uniform distribution within the room. Both converge to the true trajectory, the PF using pseudodistances is considerably faster. Looking at the error CDFs in Fig. 9 confirms the ability of the state-space methods to enhance both accuracy and also to a large extent the reliability in terms of avoiding the error floor.

An additional comparison of the proposed estimators can be found in Fig. 10 and Fig. 11. This trajectory consists of movement with longer stop phases. It can also illustrate the initialization phases of the different filters. In Fig. 10, the performance of the GSF is shown. The door positions are known via the floor plan. Therefore, $M = 3$ and the corresponding initial Gaussian position hypotheses are placed at the door positions. This leads to a very quick convergence.

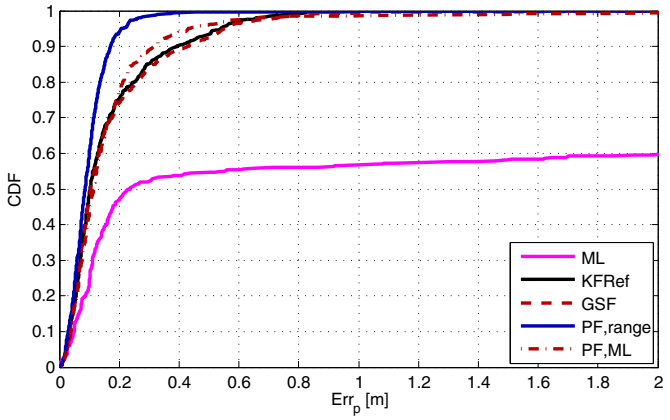


Fig. 9. CDF of the position error for the scenario shown in Fig. 8. All estimators show accurate and robust performance, even though the ML estimation shows a large percentage of outliers. For the PF using the pseudodistances, 80 % of the estimators are within 15 cm. For the other estimators, this value is at about 25 cm.

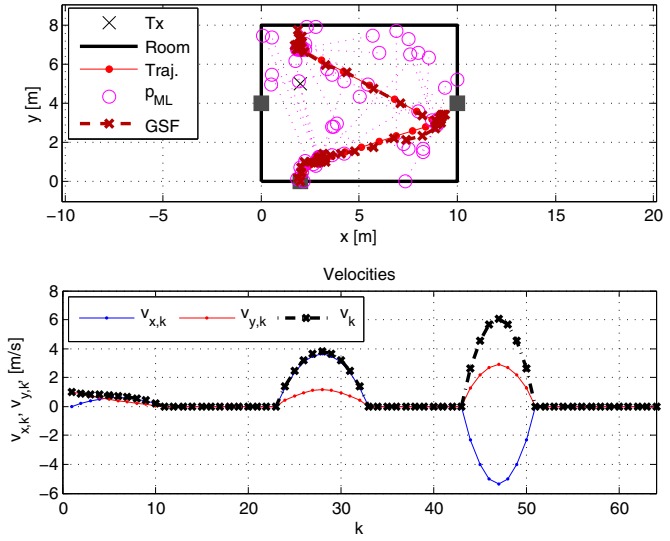


Fig. 10. Localization scenario with three doors and the Gaussian sum filter, starting point is the door at the south. The bottom plot shows the velocities for this scenario. Inbetween rather fast movements, there are also longer stop phases.

It should be mentioned, that in a case where the first few ML-estimates are outliers that come to lie in the vicinity of an incorrect initialization point, the GSF will be impaired and the convergence will take severely longer. Fig. 11 illustrates the excellent initialization capabilities of the PF, here the one with pseudodistance measurements. The comparison is between an initialization of all particles uniformly across the room and the initialization with truncated Gaussians at the doors. Both converge fast to the correct trajectory, the latter is a bit faster taking about 3 time steps while the uniformly initialized PF takes 7 time steps. A further advantage of the PF is its robustness to dynamic movement. It is difficult to optimize the fixed state noise variance parameter for KF and

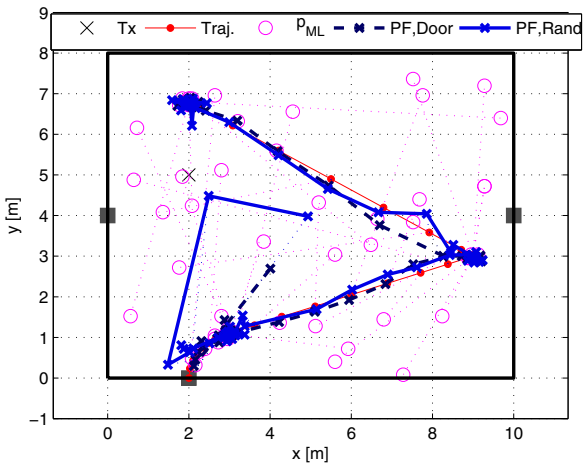


Fig. 11. Localization scenario like in Fig 10. The solid blue line shows the performance of the PF with pseudodistance measurements and $N_p = 2000$ for a random initialization of the particles uniformly across the room. The dashed line denotes the same PF where $N_p/3$ particles are initialized corresponding to a truncated bivariate Gaussian centered at each door, respectively.

GSF, because a trade-off between fast movement and stop phases has to be found. For the PF, this is not a problem due to the median operation on the posterior particles, which makes the PF also robust in stop phases.

## V. Conclusions and Future Work

We have demonstrated an indoor positioning concept exploiting the reflections of UWB radio signals with virtual anchors. Using several tracking algorithms, we have shown by simulations that this approach can deliver both accurate and robust location estimation, taking into account several possible measurement impairments. We have introduced specialized variants of popular state-space estimators to account for the impairments in our statistical models. Most importantly, we address multimodality or heavy-tail behavior in our measurement likelihood functions, which both are known to substantially impair standard state-space methods. The performance has been demonstrated by simulations for indoor pedestrian movement trajectories. Also the problem of initialization of the state-space approaches has been treated by discussing possibilities to initialize the estimators at user-chosen points of interest, e.g. room doors.

Future work will deal with the validation and extension of our statistical measurement model through the analysis of recently measured UWB channels along reference trajectories. Also, we will extend our statistical models to include the virtual anchors, their locations and their visibility in the tracking process.

## References

[1] P. Meissner, C. Steiner, and K. Witrisal, "UWB Positioning with Virtual Anchors and Floor Plan Information," in *Proc. 7th Workshop on Positioning, Navigation and Communication, WPNC 2010*, 2010.

[2] D. Simon, *Optimal State Estimation*, 1st ed. Wiley, 2006.

[3] D. Alspach and H. Sorenson, "Nonlinear Bayesian estimation using Gaussian sum approximations," *Automatic Control, IEEE Transactions on*, vol. 17, no. 4, pp. 439 – 448, aug 1972.

[4] C. Masreliez and R. Martin, "Robust bayesian estimation for the linear model and robustifying the Kalman filter," *Automatic Control, IEEE Transactions on*, vol. 22, no. 3, pp. 361 – 371, jun 1977.

[5] D. Fox, J. Hightower, L. Liao, and D. Schulz, "Bayesian Filtering for Location Estimation," *Pervasive Computing*, 2003.

[6] O. Cappe, S. Godsill, and E. Moulines, "An Overview of Existing Methods and Recent Advances in Sequential Monte Carlo," *Proceedings of the IEEE*, vol. 95, no. 5, pp. 899 –924, may 2007.

[7] M. Arulampalam, S. Maskell, N. Gordon, and T. Clapp, "A tutorial on particle filters for online nonlinear/non-Gaussian Bayesian tracking," *Signal Processing, IEEE Transactions on*, vol. 50, no. 2, pp. 174 –188, feb 2002.

[8] M. Chiani, A. Giorgetti, M. Mazzotti, R. Minutolo, and E. Paolini, "Target detection metrics and tracking for UWB radar sensor networks," in *Ultra-Wideband, 2009. ICUWB 2009. IEEE International Conference on*, 9-11 2009, pp. 469 –474.

[9] Widyawan, M. Klepal, and S. Beauregard, "A Backtracking Particle Filter for fusing building plans with PDR displacement estimates," in *Positioning, Navigation and Communication, 2008. WPNC 2008. 5th Workshop on*, march 2008, pp. 207 –212.

[10] H. Miao, K. Yu, and M. Juntti, "Positioning for NLOS Propagation: Algorithm Derivations and Cramer-Rao Bounds," *Vehicular Technology, IEEE Transactions on*, vol. 56, no. 5, pp. 2568 –2580, sept. 2007.

[11] K. Papakonstantinou and D. Slock, "Direct Location Estimation using Single-Bounce NLOS Time-Varying Channel Models," in *Vehicular Technology Conference, 2008. VTC 2008-Fall. IEEE 68th*, 21-24 2008, pp. 1 –5.

[12] V. La Tosa, B. Denis, and B. Uguen, "Maximum Averaged Likelihood Estimation Tree for Anchor-Less Localization Exploiting IR-UWB Multipaths," in *Vehicular Technology Conference (VTC 2010-Spring), 2010 IEEE 71st*, 16-19 2010, pp. 1 –5.

[13] Y. Shen and M. Win, "On the use of multipath geometry for wideband cooperative localization," in *Global Telecommunications Conference, 2009. GLOBECOM 2009. IEEE*, 30 2009-dec. 4 2009, pp. 1 –6.

[14] J. Seitz, M. Schaub, O. Hirsch, R. Zetik, T. Deissler, R. Thoma, and J. Thielecke, "UWB feature localization for imaging," in *Proc. IEEE International Conference on Ultra-Wideband ICUWB 2008*, vol. 2, Sep. 10–12, 2008, pp. 199–202, geometry/TOA based feature mapping.

[15] K. Hausmair, K. Witrisal, P. Meissner, C. Steiner, and G. Kail, "SAGE Algorithm for UWB Channel Parameter Estimation," in *COST 2100 Management Committee Meeting*, Feb. 2010.

[16] T. Santos, J. Karedal, P. Almers, F. Tufvesson, and A. Molisch, "Modeling the ultra-wideband outdoor channel: Measurements and parameter extraction method," *Wireless Communications, IEEE Transactions on*, vol. 9, no. 1, pp. 282 –290, january 2010.

[17] B. Fleury, M. Tschudin, R. Heddergott, D. Dahlhaus, and K. Ingeman Pedersen, "Channel parameter estimation in mobile radio environments using the SAGE algorithm," *Selected Areas in Communications, IEEE Journal on*, vol. 17, no. 3, pp. 434 –450, mar 1999.

[18] A. F. Molisch, "Ultra-wide-band propagation channels," *Proc. IEEE*, vol. 97, no. 2, pp. 353–371, Feb. 2009.

[19] T. Liu, P. Bahl, and I. Chlamtac, "Mobility modeling, location tracking, and trajectory prediction in wireless ATM networks," *Selected Areas in Communications, IEEE Journal on*, vol. 16, no. 6, pp. 922 –936, aug 1998.

[20] B. Dong and X. Wang, "Adaptive Mobile Positioning in WCDMA Networks," *EURASIP Journal on Wireless Communications and Networking*, vol. 3, pp. 343–353, 2005.

[21] P. Georgiou, P. Tsakalides, and C. Kyriakakis, "Alpha-stable modeling of noise and robust time-delay estimation in the presence of impulsive noise," *Multimedia, IEEE Transactions on*, vol. 1, no. 3, pp. 291 –301, sep. 1999.

[22] G. Tsihrintzis and C. Nikias, "Incoherent receivers in alpha-stable impulsive noise," *Signal Processing, IEEE Transactions on*, vol. 43, no. 9, pp. 2225 –2229, sep 1995.

[23] T. S. Ferguson, "A representation of the symmetric bivariate cauchy distribution," *The Annals of Mathematical Statistics*, vol. 33, no. 4, pp. pp. 1256–1266, 1962. [Online]. Available: http://www.jstor.org/stable/2237984

[24] S. Kay, *Fundamentals of Statistical Signal Processing: Estimation Theory*. Prentice Hall Signal Processing Series, 1993.